



Research Article

Research on Slug Flow Elimination Method Based on Kinetic Energy Conversion

Ruiquan Liao ^{1,2,3,4}, Donghui Zhou,^{2,3,4} Zhihui Wang,^{2,3,4} Weixia Yang,⁵
and Xingkai Zhang ^{1,2,3,4}

¹Key Laboratory of Exploration Technologies for Oil and Gas Resources (Yangtze University), Ministry of Education, Wuhan, China 430100

²Petroleum Engineering Institute of Yangtze University, Wuhan, China 430100

³Laboratory of Multiphase Pipe Flow, Gas Lift Innovation Center, China National Petroleum Corp., Wuhan, China 430100

⁴Key Laboratory of Drilling and Production Engineering for Oil and Gas, Wuhan, China 430100

⁵Jinchang PetroChina Kunlun Gas Co., Ltd., Jinchang, China 737100

Correspondence should be addressed to Xingkai Zhang; zhangxingkai001@163.com

Received 19 October 2022; Revised 7 November 2022; Accepted 24 November 2022; Published 30 January 2023

Academic Editor: Ze Wang

Copyright © 2023 Ruiquan Liao et al. This is an open access article distributed under the Creative Commons Attribution License, which permits unrestricted use, distribution, and reproduction in any medium, provided the original work is properly cited.

Slug flow is one of the most common flow patterns in the petrochemical industry. It will affect the normal operation of oil well surface pipelines and connected equipment, especially gas well multiphase flowmeters. The extant slug flow traps are complex in structure and limited in application sites. To reduce the influence of slug flow on gas-liquid two-phase measurement, a slug flow elimination device is designed based on the kinetic energy conversion method. The gas-liquid two-phase flow law inside the device and its energy loss are investigated using a combination of indoor experiments and numerical simulations. This study evaluates the device's working performance, including the flow pattern, pressure fluctuation, velocity distribution, and energy loss. The results show that the flow rate and pressure fluctuation of the gas-liquid two-phase flow are weakened after the device. And the flow pattern changes from intermittent slug flow to gas-liquid continuous flow. The pressure drop calculation method for the device is developed based on the share of different structures in the total pressure drop, with a prediction error of 20%. The slug elimination device is designed to provide a flow pattern basis for metering equipment, improve metering accuracy, and further promote the development of multiphase metering technology.

1. Introduction

The fluids produced from oil wells may be a gas-liquid two-phase flow in many cases. Slug flow is a common gas-liquid two-phase flow pattern. Slug flow will affect the stable operation of the oil well surface pipeline and the equipment connected to the pipeline. In particular, slug flow will cause large measurement errors in the real-time measurement of oil well production [1]. A large number of studies have been conducted to investigate the kinematic characteristics of slug flow [2–5]. Based on the existing theories, the optimal method to reduce or eliminate the slug flow is sought [6]. Meng et al. [7] and Zheng et al. [8] installed a cyclone

upstream of the gas-liquid measurement device to eliminate the slug so that the flow through the measurement device is annular. They concluded that the cyclone can force the downstream flow pattern into an annular flow and obtained a stable differential pressure, thus obtaining high measurement accuracy. Passive section slug control can also be achieved by using many devices or techniques, commonly installing flow pattern adjusters [9, 10], multiple riser combinations [11], gas lift method [12], bubble crushers [13], mixing devices [14], and slug flow traps [15], etc. In general, according to the site production needs, different types of slug flow elimination devices can be chosen [16]. If the slug flow can be effectively eliminated, it will not only provide a good

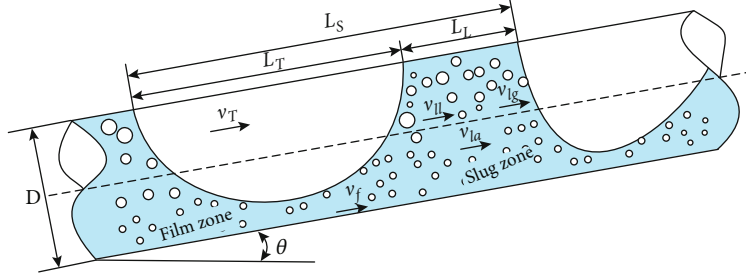


FIGURE 1: Geometric model of the slug flow in the inner section of the slightly inclined pipe.

flow basis for gas-liquid measurement but also improve the stability of equipment operation [17, 18].

To eliminate the measurement error caused by a sudden change in the flow pattern, the experimental study of the slug flow elimination method under different working conditions is the most convincing. Experimental studies are limited to some extent due to the disadvantages such as the high cost of experimental equipment and low reusability. Researchers began to seek more accurate and predictive tools for the study of gas-liquid two-phase flow laws [19]. Among them, Computational Fluid Dynamics (CFD) methods are coming into the researchers' view, and they will be a valuable addition to the toolbox [20].

The purpose of this study is to eliminate or weaken the slug flow and provide a stable flow pattern for gas-liquid two-phase measurements while increasing the stability of the instrument operation. Based on the principle of kinetic energy conversion and turbulent diffusion [21], a new slug flow elimination method is put forward to change the distribution pattern of gas and liquid phases [22]. This method can effectively reduce the slug flow frequency and achieve the purpose of weakening or eliminating the slug flow. The performance of the slug flow elimination device is tested by experimental and numerical simulation, and the pressure drop calculation model of the device is also established.

2. Model Building and Methodology

2.1. Slug Flow Model. When the gas-liquid two-phase flow flows through the horizontal- or upward-inclined pipeline, the liquid moves forward under the action of a pressure gradient to overcome gravity and friction. When the pressure gradient or gas-carrying role is large enough, the liquid has a large kinetic energy and can flow together with the gas. On the contrary, the impact of gravity and friction will move the liquid behind the gas, causing the liquid to accumulate in the pipe, and then generating hydraulic slug flow. Therefore, if the energy of the liquid is increased by certain means, the slug flow can be eliminated.

As shown in Figure 1, the total length of a hydraulic slug flow unit is L_s , which mainly consists of a liquid film zone and a liquid slug zone. Assume that the length of the liquid slug zone is L_L and the length of the liquid film zone is L_T , where the liquid film zone consists of Taylor bubbles and liquid film. The hydraulic section slug flow is accompanied

by the accumulation of the liquid phase at the head of the slug and the loss of the liquid phase at its tail during the movement.

Taking the slug flow unit as the object of study, the continuity equation is established based on the conservation of mass of the slug flow per unit of time.

$$\text{Liquid} : \frac{v_{sl}\rho_l}{e} = v_{ll}t_s H_{ls}\rho_l + v_f t_f H_{lf}\rho_l, \quad (1)$$

$$\text{Gas} : \frac{v_{sg}\rho_g}{e} = v_{lg}t_s(1 - H_{ls})\rho_g + v_T t_f(1 - H_{lf})\rho_g, \quad (2)$$

where v_{sl} and v_{sg} represent the superficial velocity of liquid and gas, respectively, m/s. v_{ll} and v_f represent the liquid phase velocity in the liquid slug and liquid film zones, respectively, m/s. H_{ls} and H_{lf} represent the liquid holdup in the liquid slug and liquid film zones, respectively, dimensionless. e is the frequency of the slug flow, Hz. v_{lg} and v_T are the bubble velocity and Taylor bubble velocity in the liquid slug zone, respectively, m/s. ρ_l and ρ_g represent the density of the liquid and gas, respectively, kg/m^3 . t_s and t_f represent the time for the liquid slug and Taylor bubble to pass a point, respectively, s.

$$t_s = \frac{L_L}{v_{ll}}, \quad (3)$$

$$t_f = \frac{L_f}{v_f}. \quad (4)$$

Substituting Equations (3) and (4) into Equations (1) and (2), respectively, we get

$$\frac{v_{sl}}{e} = \frac{L_L H_{ls} v_{ll}}{v_{la}} + L_f H_{lf}, \quad (5)$$

$$\frac{v_{sg}}{e} = \frac{L_L v_{lg}}{v_{la}}(1 - H_{ls}) + \frac{L_f}{v_f}(1 - H_{lf})v_T. \quad (6)$$

The Taylor bubble motion process causes the interconversion of the liquid slug and liquid film zones, and in the steady state, the mass exchange is

$$H_{ls}(v_T - v_{ll}) = H_{lf}(v_T - v_{ll}). \quad (7)$$

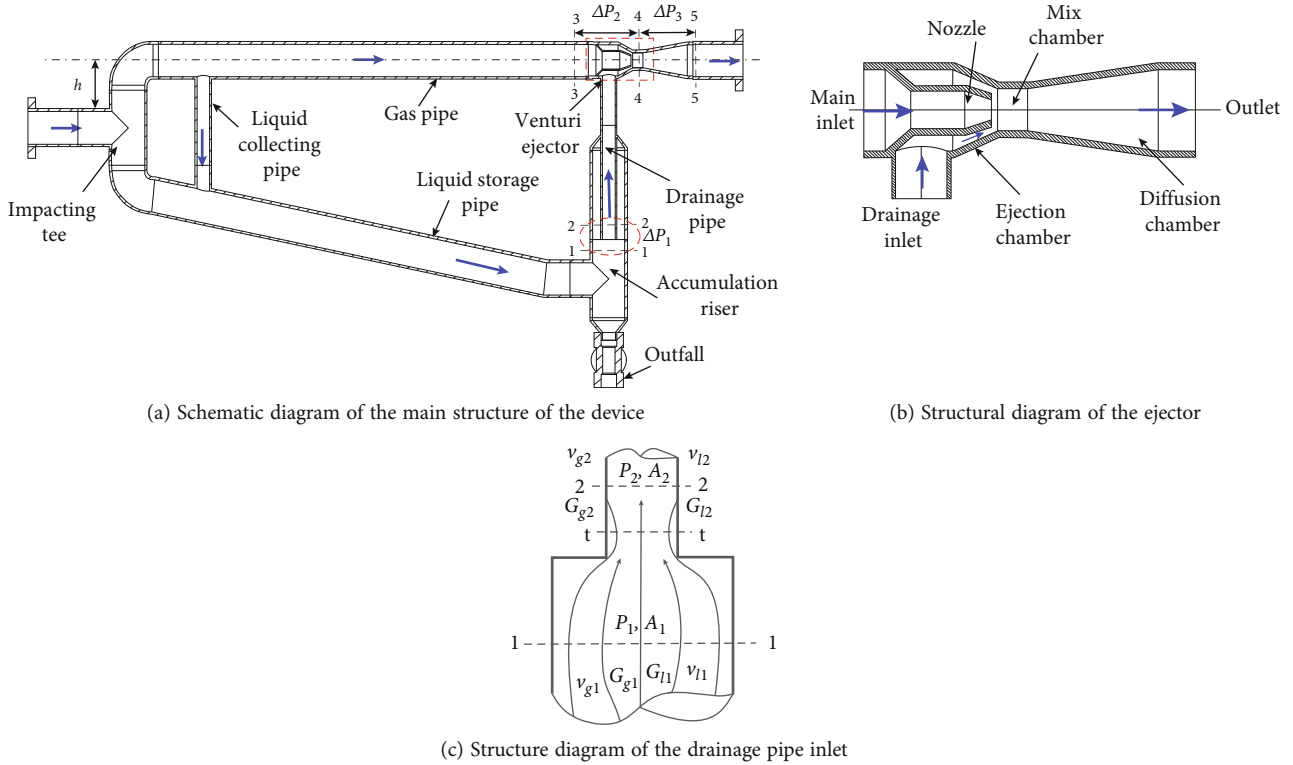


FIGURE 2: Schematic design of the main structure of the slug flow elimination device (the blue arrow is the flow direction).

A certain amount of liquid holdup is the basic condition for the formation of slug flow. The liquid holdup in the liquid slug zone is much larger than that in the liquid film zone in the slug flow unit. The liquid holdup of the slug is calculated according to the relationship proposed by Gregory [23], namely,

$$H_{ls} = \frac{1}{1 + [v_m/8.66]^{1.39}}. \quad (8)$$

The velocity of the mixture (v_m) in the slug flow unit can be expressed as

$$v_m = v_{sl} + v_{sg}. \quad (9)$$

2.2. Structure and Working Principle. The elimination device designed and processed in this study mainly consists of an impacting tee, an ejector, a liquid accumulation riser, a liquid storage pipe, and a gas pipe, and the structure is shown in Figure 2(a). Among them, the main function of the impacting tee is to separate the liquid slug area and liquid film area of the slug flow unit, so that the gas-liquid two phases are reorganized at the Venturi throat. When the slug flow passes through the inlet impacting tee, the kinetic energy of the liquid along the axial direction disappears and flows into the liquid storage pipe by its gravity. The impacting tee has little effect on the gas superficial velocity, and the gas in the Taylor bubble enters the horizontal gas pipe. The role of the ejector is to convert part of the gas velocity into the liquid. The gas velocity increases and pres-

sure decrease as it flows through the nozzle. Low pressure draws the liquid in the accumulation riser into the mix chamber (Figure 2(b)), achieving gas-liquid kinetic energy exchange so that the liquid velocity increases. By recombining the gas-liquid phases through the ejector, the energy distribution of each phase in the pipe and the liquid content distribution in the cross-section are changed. When the liquid content of the treated section does not meet the conditions for the formation of slug flow [24], the slug disappears.

3. Experimental System

3.1. Experimental Procedure. Water and air are used as media for the experiment. The experimental fluid is supplied through a water pump and an air compressor. The high-pressure gas in the storage tank is dried and processed into the slug flow elimination device. The separated gas is directly discharged into the air, and the water is recycled. The experimental flow is as shown in Figure 3. In this experiment, an “L” riser is set at the inlet to simulate the slug flow, so that the flow pattern entering the separation device is a slug flow. The experimental setup is shown in Figure 4(d).

3.2. Experimental Equipment. The liquid flow rate is given by adjusting the pump inverter to change the liquid flow rate into the mixer. The gas flowmeter used in this experiment is a thermal gas mass flowmeter with a measurement range of 5 m³/h to 400 m³/h and an accuracy of $\pm 1.5\%$. The liquid flow rate is measured by a Coriolis force mass flowmeter with a range of 0 to 1.5 kg/s and an accuracy of $\pm 0.1\%$. Pressure sensors are installed at the inlet and outlet of the

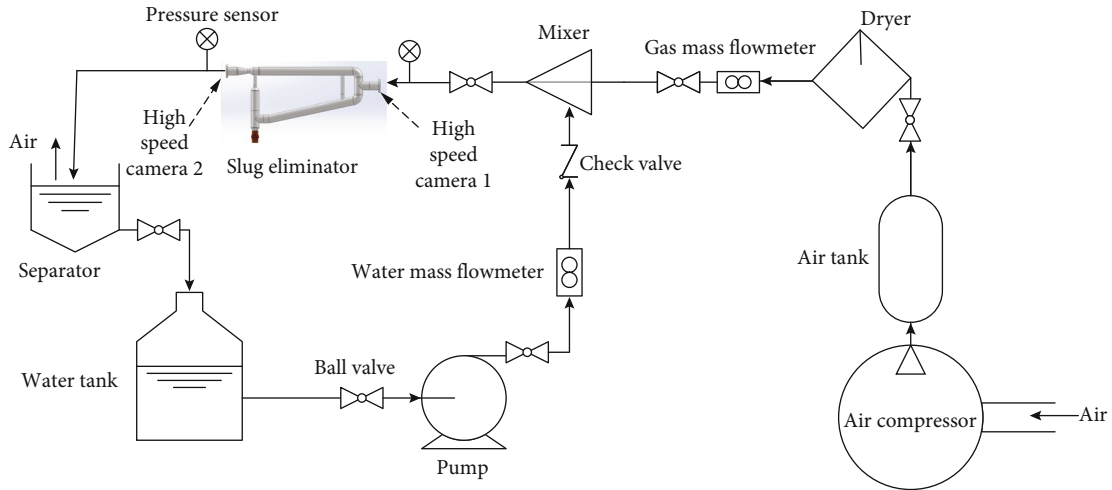


FIGURE 3: Experimental flow chart.

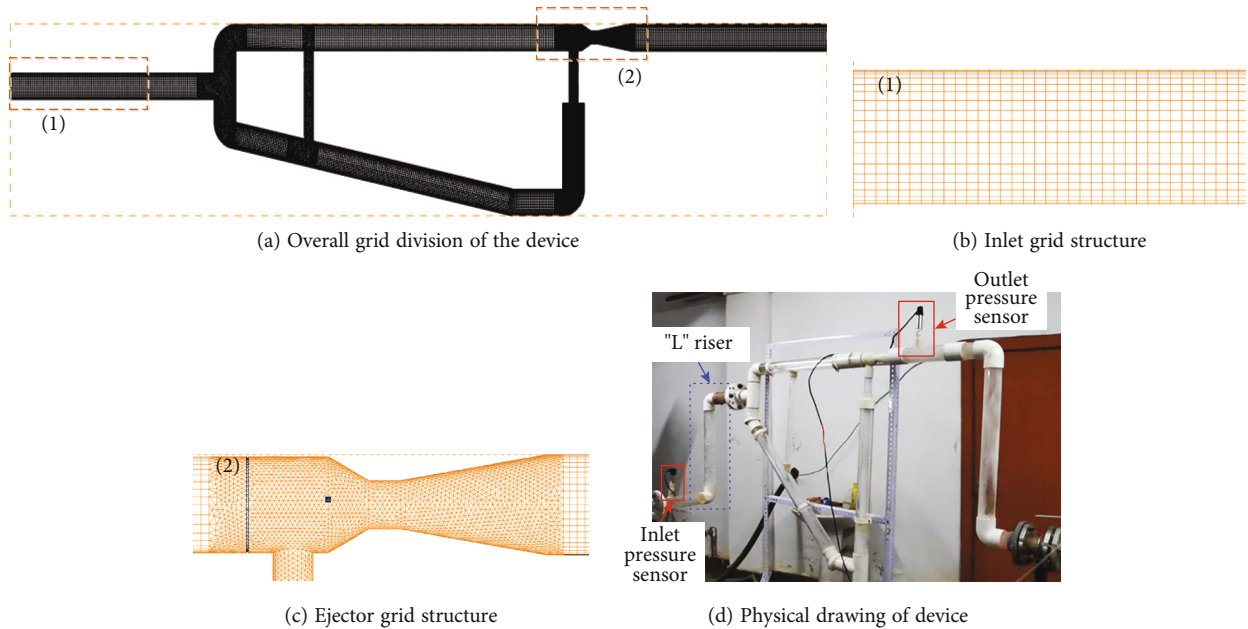


FIGURE 4: Physical model and grid structure (the blue dotted box is the "L" riser).

elimination device to record the pressure change before and after entering the device, to judge the effect of slug flow elimination. The pressure sensors at the inlet and outlet have a range of 0~0.6MPa and an accuracy of $\pm 0.1\%$. The output of the flowmeter and differential pressure sensor is a 4-20 mA current signal, and all parameters are collected and stored using an NI PCI-6220 64-bit multifunctional data acquisition card with a 200 Hz data acquisition frequency.

3.3. Numerical Simulation. Slug flow is an intermittent flow between gas-liquid phases and requires specific operating conditions to be formed. Therefore, this simulation utilizes the user-defined function (UDF) to customize the gas-liquid flow at the inlet to ensure that the two phases can form a slug flow before entering the device. According to

the experimental findings, the loading and unloading processes of the compressor lead to a sinusoidal variation of the gas flow [25]. So the inlet mass flow curve is defined as a sinusoidal fluctuation law during the numerical simulation. The numerical simulation results are verified by experiments with the same structure.

3.4. Physical Model and Grid. When building the physical model, the inlet and outlet pipe lengths were increased to observe the slug flow elimination effect. The inner diameters of both outlet and inlet pipes are 60 mm, the inner diameters of both descending and inducing pipes are 25 mm, and the throat diameter ratio of the ejector is 0.4. To improve the mesh quality and enhance the calculation accuracy, the structure is first divided into blocks, and the structured meshing method is used for the regular structure. The

ejector and the impacting tee use the tetrahedral meshing method, and the mesh structures are shown as follows in Figures 4(a)–4(c).

3.5. Multiphase Flow Model. The VOF model is chosen for this simulation to simulate the gas-liquid distribution law with the following control equation.

$$\frac{\partial \alpha_q}{\partial t} + \vec{v} \cdot \nabla \alpha_q = \frac{S \alpha_q}{\rho_q}. \quad (10)$$

By default, the source term at the right of Eq. (10) is zero, except when a constant or a user-defined mass source is specified for each phase. The volumetric ratio equation is not solved for the main phase. The calculation of the volume ratio for the main phase is based on the following constraint.

$$\sum_{q=1}^n \alpha_q = 1. \quad (11)$$

Solving for a single momentum equation over the entire zone, the resulting velocity field is shared by all phases. As shown below, the momentum equation depends on the volume ratio of all phases of ρ and μ .

$$\frac{\partial}{\partial t} (\rho \vec{v}) + \nabla \cdot (\rho \vec{v} \vec{v}) = -\nabla p + \nabla \cdot [\mu (\nabla \vec{v} + \nabla \vec{v}^T)] + \rho \vec{g} + \vec{F}. \quad (12)$$

In this simulation, the gas is used as the primary phase and the liquid as the secondary phase, and the density in each grid cell is calculated using the following equation.

$$\rho = \rho_g \alpha_q + \rho_l (1 - \alpha_q), \quad (13)$$

where \vec{v} is the velocity of the fluid, α_q is the q -th phase volume fraction, ρ_q is the q -th density, p is the static pressure, μ is the fluid's dynamic viscosity, and \vec{F} is the surface tension between the two phases.

3.6. Turbulence Model. The RNG $k - \varepsilon$ model is capable of simulating moderately complex flows such as jet impingement, separated flows, secondary flows, and cyclonic flows. The model is derived from the transient N - S equation using the mathematical method of the “renormalization group.” The resolvability is converted from the standard $k - \varepsilon$ model, and new functions or terms appear in the equations, whose turbulent kinetic energy and dissipation rate equations are

$$\rho \frac{Dk}{Dt} = \frac{\partial}{\partial x_i} \left[(\alpha_k \mu_{\text{eff}}) \frac{\partial k}{\partial x_i} \right] + G_k + G_b - \rho \varepsilon - Y_M, \quad (14)$$

$$\rho \frac{D\varepsilon}{Dt} = \frac{\partial}{\partial x_i} \left[(\alpha_\varepsilon \mu_{\text{eff}}) \frac{\partial \varepsilon}{\partial x_i} \right] + C_{1\varepsilon} \frac{\varepsilon}{k} (G_k + C_{3\varepsilon} G_b) - C_{2\varepsilon} \rho \frac{\varepsilon^2}{k} - R, \quad (15)$$

where G_k is the turbulent kinetic energy due to the velocity gradient; G_b is the turbulent kinetic energy due to buoy-

ancy; Y_M is the fluctuation due to the diffusion of the transition in compressible turbulence; $C_{1\varepsilon}$, $C_{2\varepsilon}$, and $C_{3\varepsilon}$ are constants; and α_k and α_ε are the inverse of the effective turbulent Prandtl number for the turbulent kinetic energy k and the dissipation rate ε , respectively.

3.7. Boundary Conditions. The inlet and outlet boundary types are set as the mass flow inlet and pressure outlet, respectively. The inlet pressure is 0.1 MPa, and the inlet mass flow rate is assigned by UDF. The turbulence definition method selects the turbulence intensity and hydraulic diameter; the no-slip wall condition is used; i.e., the wall velocity is 0. The gas-liquid surface tension is set to 0.0072 N/m. The parameters such as phase content, pressure, and phase velocity in the flow direction are recorded during the simulation.

4. Results and Discussion

4.1. Flow Pattern. Flow pattern variation is the main cause of pressure in the pipe [26]. As Figure 5(a) shows, the inlet is a slug flow, and bubbles are found in the liquid slug in the slug flow unit. The closer to the end of the liquid slug, the larger the bubble is. This is caused by the pressure between the liquid film and the liquid slug becoming smaller. When the slug flow enters the device, a large amount of liquid is initially separated into the descending pipe under the small gas-liquid ratio condition, and a small amount of liquid is carried to the horizontal pipe by the gas. The preliminary separation of the gas and liquid is obvious, in which a small amount of liquid in the gas pipe flows into the liquid collection pipe through the descending pipe. The gas imparts kinetic energy to the liquid in the mix chamber of the ejector, which improves the velocity of the liquid and reduces the accumulation of liquid in the riser. After passing through the elimination device, the liquid slug and Taylor bubble are separated, and the flow pattern formed after the second mixing is as Figure 5(b) shows. From Figure 5(b), it can be seen that the flow pattern at the outlet has changed from slug flow to transition flow and gradually transformed to annular flow. Due to gravity, the liquid phase at the outlet is deposited at the bottom of the pipe, forming a small wave, and a fine liquid flow is formed around the pipe wall, which temporarily fails to form a complete liquid film.

The liquid holdup is one of the main variables describing the slug flow. Therefore, the magnitude of the liquid holdup not only affects the pressure fluctuation but will also determine the slug flow elimination effect. According to the Gregory et al. [27] study, the liquid holdup of the pipe cross-section capable of slug flow is 48%. The experimental results show that when the gas-liquid ratio is greater than $380 \text{ m}^3/\text{m}^3$, it is difficult to form slug flow in the pipe. However, a large gas-liquid ratio still leads to a liquid-phase impact on the impacting tee and a significant wave pattern in the outlet pressure.

When the kinetic energy of the gas is small, it cannot pump the liquid in the accumulation riser in time, causing it to accumulate (Figure 6(a)). When the gas cannot continuously transfer its kinetic energy to the liquid, the liquid

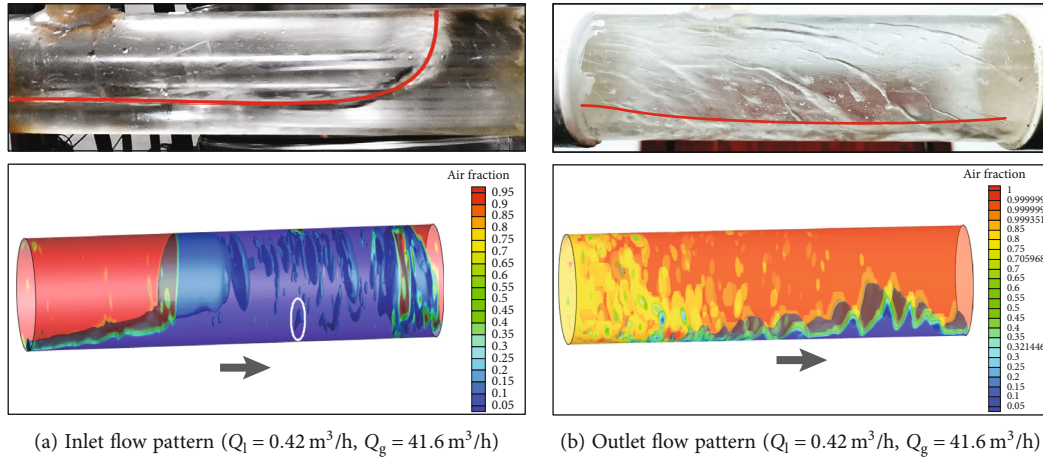


FIGURE 5: Fluid motion at the inlet and outlet of the experimental setup.

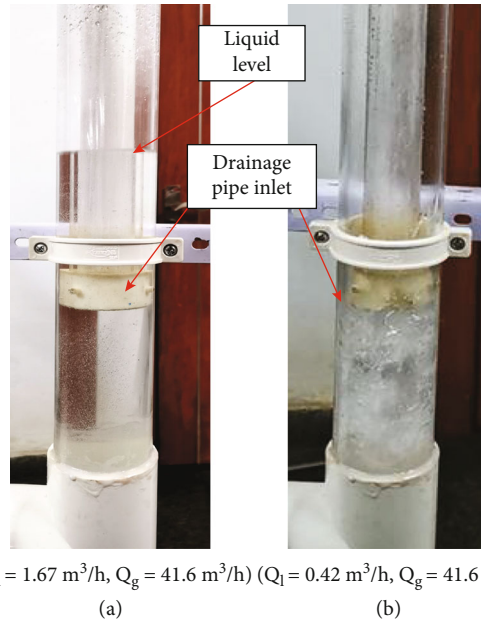


FIGURE 6: Liquid state of the accumulation riser with a different gas-liquid ratio.

entering the priming chamber appears to oscillate at the inlet of the drainage pipe (Figure 6(b)). Figure 7 shows the distribution of the liquid phase at $t = 2.2 \text{ s}$ under different gas-liquid ratio conditions. As the gas-liquid ratio gradually increases, the initial separation effect of the impacting tee on the two-phase gas-liquid decreases, and a vortex is generated at the elbow. More liquid enters the gas pipe. The liquid phase entering the gas pipe makes the flow rate at the nozzle fluctuate, and the energy conversion between the gas and liquid phases is then affected. When the gas-liquid ratio is greater than $120 \text{ m}^3/\text{m}^3$, a complete slug flow is not formed at the inlet due to the reduced liquid content in the pipe. It can be seen from the outlet pressure curve that the gradual increase of the gas-liquid ratio increases the outlet pressure amplitude. Due to the small liquid content rate, a full pipe flow cannot be formed in the accumulation riser, and the intermittent supply of liquid from the riser to the inlet pipe results. Therefore, the pressure fluctuations generated at a

gas-liquid ratio greater than $120 \text{ m}^3/\text{m}^3$ cannot be used to define the applicability of the device.

4.2. *Pressure Fluctuation.* From the experimental phenomena, it is clear that the slug flow pressure signal has the following characteristics.

- (1) The pressure fluctuation time in the liquid film area is long, the amplitude is small, and there are obvious fluctuations in the pressure rise phase with a step-up pattern
- (2) The pressure amplitude in the liquid slug area is large, has a short duration, and shows a vertical wave, and the pressure reaches the highest point when a precipitous drop occurs [25].

Combining Figures 5 and 8(a), it can be seen that the pressure at the outlet depends on the various flow patterns.

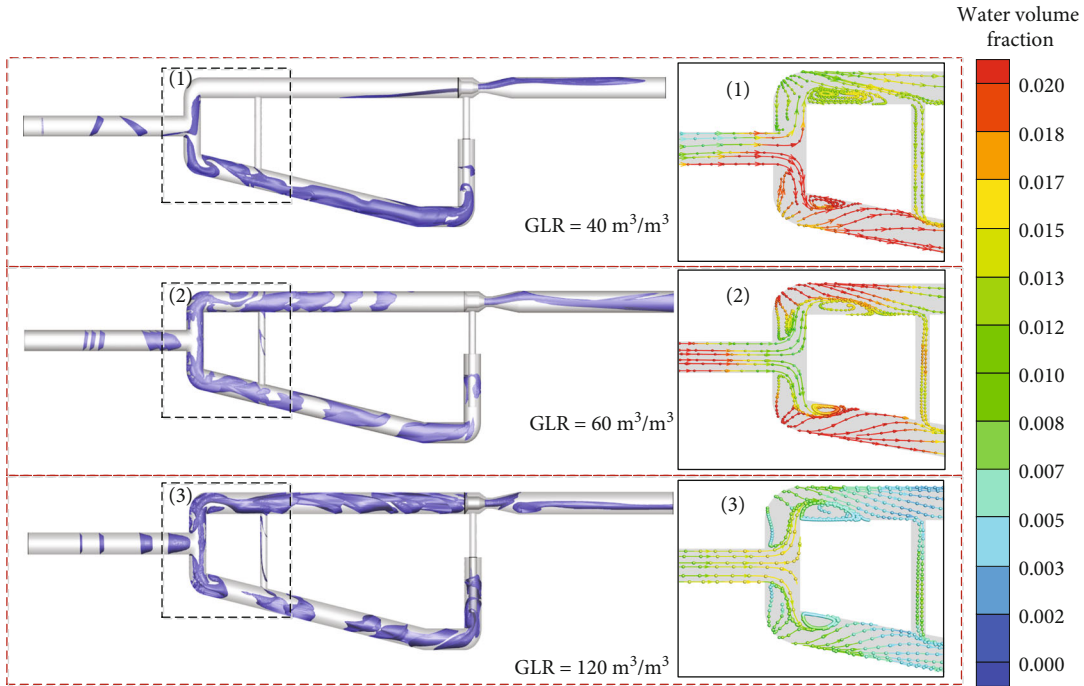


FIGURE 7: Gas-liquid distribution under different gas-liquid ratios ($t = 2.2$ s).

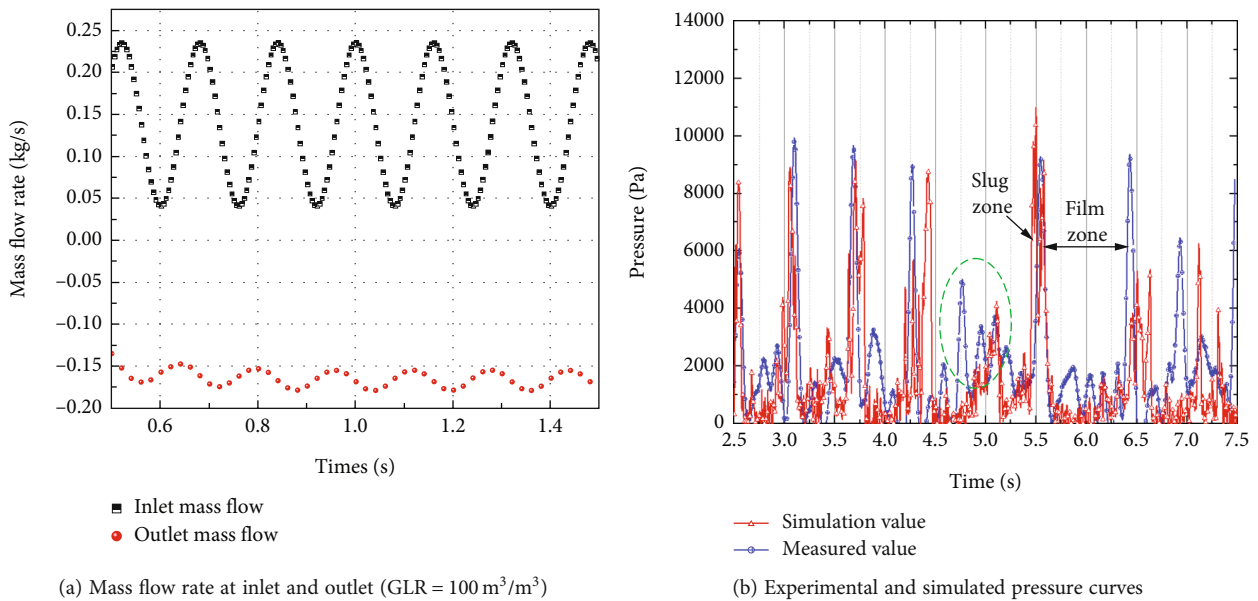


FIGURE 8: Variation of flow and pressure at the inlet and outlet.

Under non-slug flow conditions, both mass flow and pressure tend to stabilize, which can further improve the accuracy of the gas-liquid two-phase measurement device and its stability. From Figure 8(b), which shows various patterns of the inlet pressure, it can be seen that the various patterns of simulated and measured pressures are almost the same at the same time nodes. The two have a high degree of agreement. Due to the loading and unloading of the air compressor during the experiment, which leads to the unstable gas-liquid flow, it will

form as shown in Figure 8(b) (green dashed line). That is, the measured pressure value occasionally shows large fluctuations at the position of the trough, and the pressure measurement is slightly higher than that of the simulated value. Comparing the variation laws of pressure, flow pattern, and other parameters under experimental and numerical simulation conditions, respectively, it is verified that the numerical simulation method can accurately describe the gas-liquid two-phase flow pattern and its motion law.

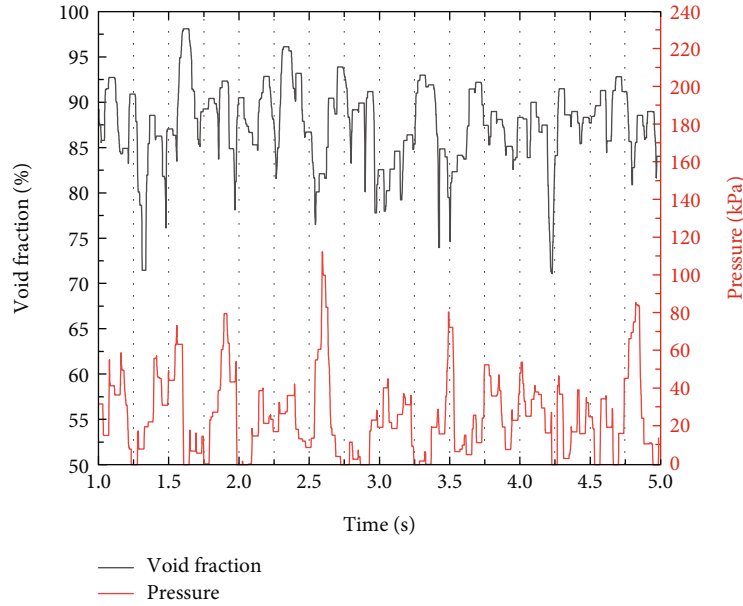


FIGURE 9: Variation curve of cross-sectional void ratio and pressure.

The relationship between the void fraction and pressure at the cross-section 400 mm from the inlet before the liquid slug enters the impacting tee ($GLR = 60 \text{ m}^3/\text{m}^3$) was simulated in this study, as shown in Figure 9. The graph shows that the pipe pressure reaches its maximum value when the void fraction reaches its minimum value, i.e., when the cross-sectional liquid content is at its maximum. When the cross-sectional liquid content increases, the pressure starts to build up in the Taylor bubble at the moment when the liquid slug blocks the gas passage. When the pressure at the end of the slug is greater than the pushing force required for the movement of the slug, the slug is discharged. At this point, the Taylor bubble acts as a “piston” and pushes the liquid slug to move. Combined with Figure 9, it can be seen that the larger the gas-liquid ratio, the larger the void ratio, and the smaller the average cross-sectional liquid content, the smaller the pressure in the pipe and the smaller the amplitude of pressure fluctuation.

Combined with the flow pattern variation at the inlet and outlet, it shows that the magnitude of the pressure fluctuation depends on the velocity of the slug flow, and the length of the slug flow determines the duration of the pressure peak. From the results of Figure 10, it can be seen that the higher the liquid phase flow rate, the higher the pressure and the greater the amplitude of its fluctuation under the same gas flow rate. The smaller the gas-liquid ratio, the longer the duration of the pressure wave. The pressure fluctuations at the inlet and outlet have obvious differences. Among them, the high-frequency pressure signal at the inlet shows obvious slug flow characteristics, but the inlet slug flow pressure signal occasionally shows abnormal fluctuations at the trough during the experiment due to the influence of compressor loading (Figure 10(a) marked by a red solid line). During the experiment, it was found that when the liquid slug reached the top of the riser, the pressure reached a peak at that time. When the slug is discharged momentarily, the pressure suddenly decreases. As the gas-liquid ratio gradu-

ally decreases, the liquid slug stagnates at the riser and a small amount of liquid then flows back, causing the pressure signal at the inlet to fluctuate at the crest, as shown in Figures 10(b) and 10(c) marked by the red solid line. Combined with Figure 8(a), which shows the mass flow rate variation law, it can be seen that the stability of the outlet pressure depends on whether its mass flow rate is stable.

4.3. Velocity Distribution. From the internal streamline diagram of the ejector (Figure 11), it can be seen that the velocity is smaller near the pipe wall and is larger in the center where the liquid content is small. The velocity before entering the ejector is about 1.15 m/s and reaches 13.41 m/s inside the mix chamber ($GLR = 40 \text{ m}^3/\text{m}^3$). The sudden increase in velocity caused a sharp drop in pressure in the mix chamber due to the reduced-flow cross-section of the nozzle. To maintain the local pressure balance, the pressure in the induced chamber also decreases simultaneously. The liquid in the accumulation riser is pumped into the mix chamber by negative pressure and then enters the expansion pipe after being accelerated by high-speed gas, forming a non-slug flow downstream. As the gas-liquid ratio increases, the flow rate in the mix chamber gradually increases, and the suction force continues to increase.

Due to the existence of friction between the liquid and the pipe wall, the flow rate gradually decreases from the center to the wall. Among them is the location of the thin layer near the inner wall, which is a thin layer of resistance; this thin layer is called the boundary layer. In the flow through the throat, the fluid increases the velocity and decreases the pressure, maintaining the original surface layer. Downstream of the throat, the flow area increases, the kinetic energy of the fluid is converted into pressure energy, and the boundary layer is subject to the force of the opposite direction of the mainstream, resulting in fluid backflow. Beyond the boundary layer of the fluid to maintain the

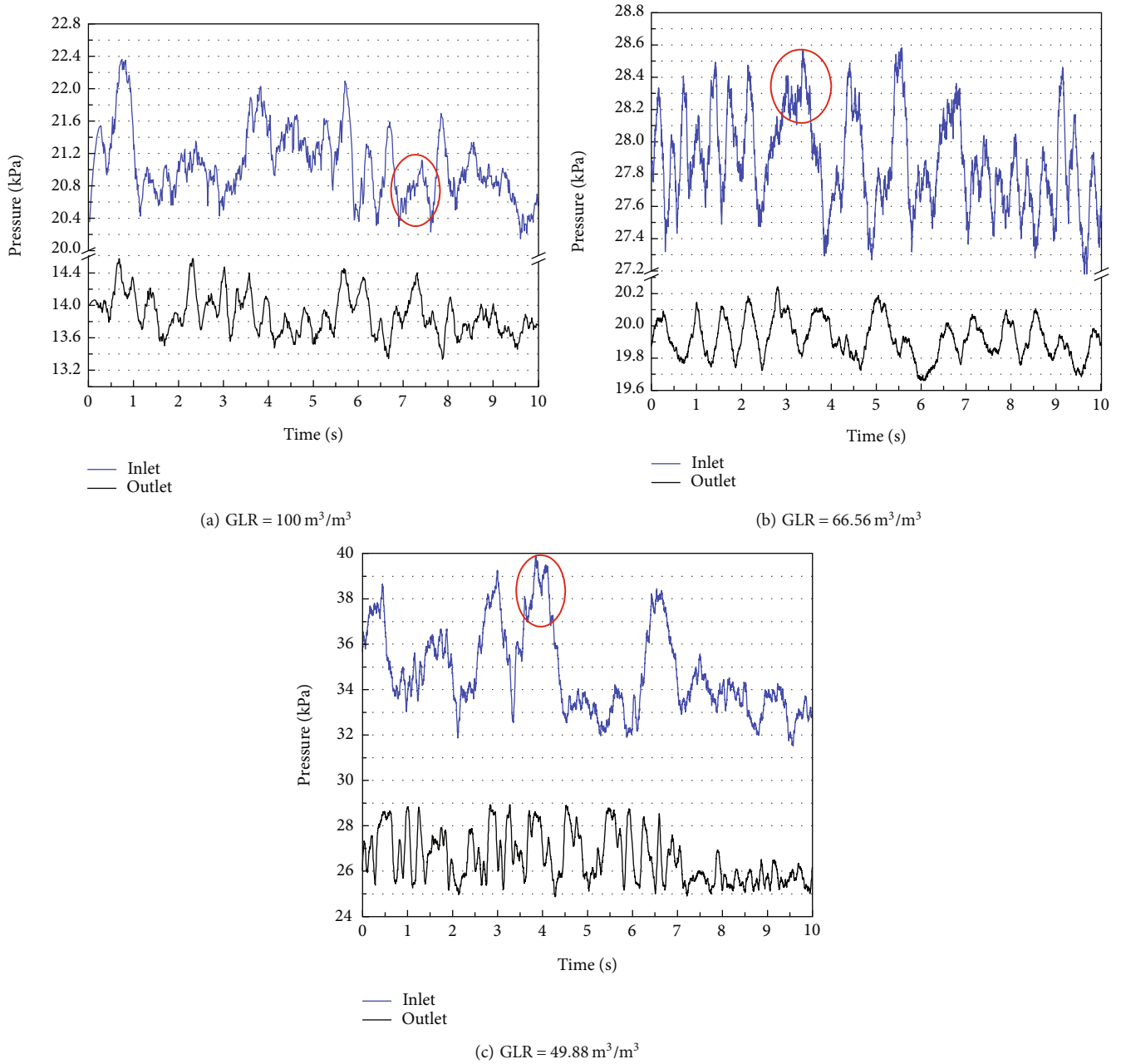


FIGURE 10: Pressure fluctuation curve of the inlet and outlet with a different gas-liquid ratio.

original direction of advance, the formation of the vortex phenomenon as shown in Figure 8 results in the separation of the boundary layer.

4.4. Pressure Drop Model. Through experiments and simulations, it can be seen that the pressure loss generated by this device mainly comes from the ejector, the inlet of the drainage pipe, the impacting tee, and the heavy pressure drop. The total pressure drop of the slug flow elimination device is

$$\Delta P = \Delta P_o + \Delta P_1 + \Delta P_v + \Delta P_h, \quad (16)$$

where ΔP_o is the pressure drop generated by the impacting tee, kPa. ΔP_1 is the pressure drop generated at the inlet

of the drainage pipe, kPa. ΔP_v is the pressure drop generated by the ejector, kPa. ΔP_h is the repositioning pressure difference from the height difference, kPa.

Under the same conditions of the gas flow rate, the total pressure drop increases gradually as the liquid flow rate increases. As Figure 12(a) shows, the liquid-phase flow rate is related to the total pressure drop. According to the study, it is known that the frictional pressure drops upstream and downstream of the Venturi throat are equal under the condition of symmetry between the constriction and expansion sections [28]. In this study, due to the complex structure of the ejector, the differential pressure generated in the convergent section is significantly larger than that in the divergent section (as Figure 12(b)). From Figure 12(b), it can be seen

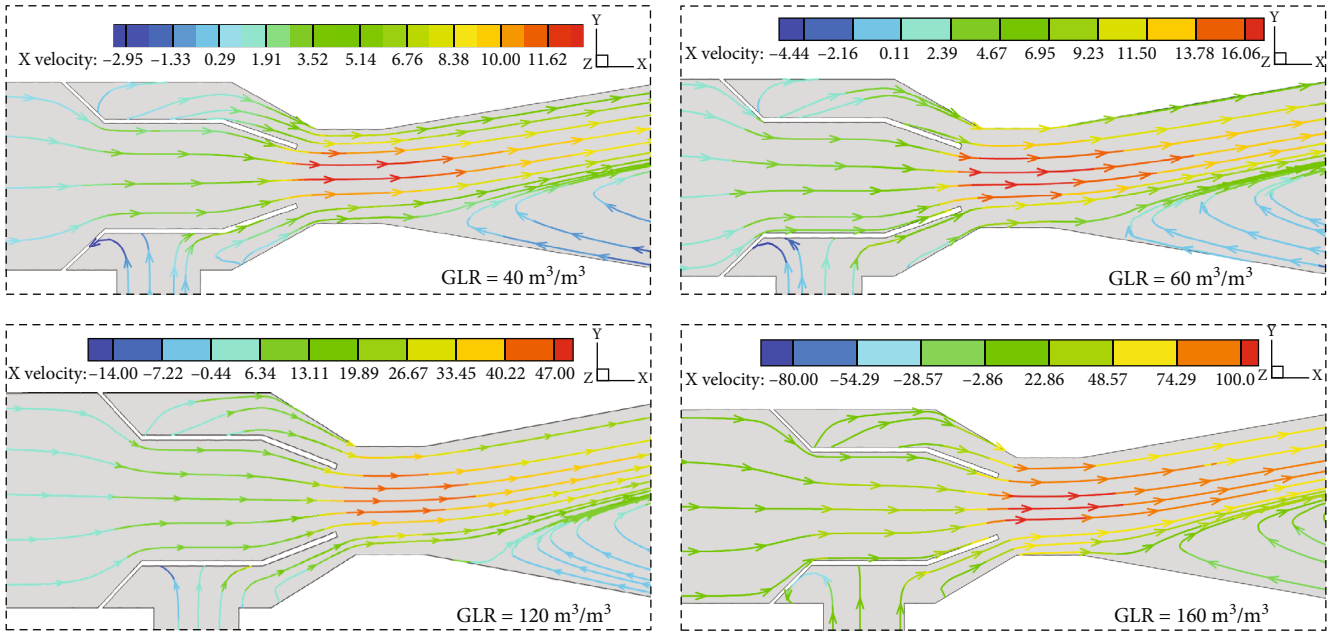


FIGURE 11: Streamline diagram of the ejector.

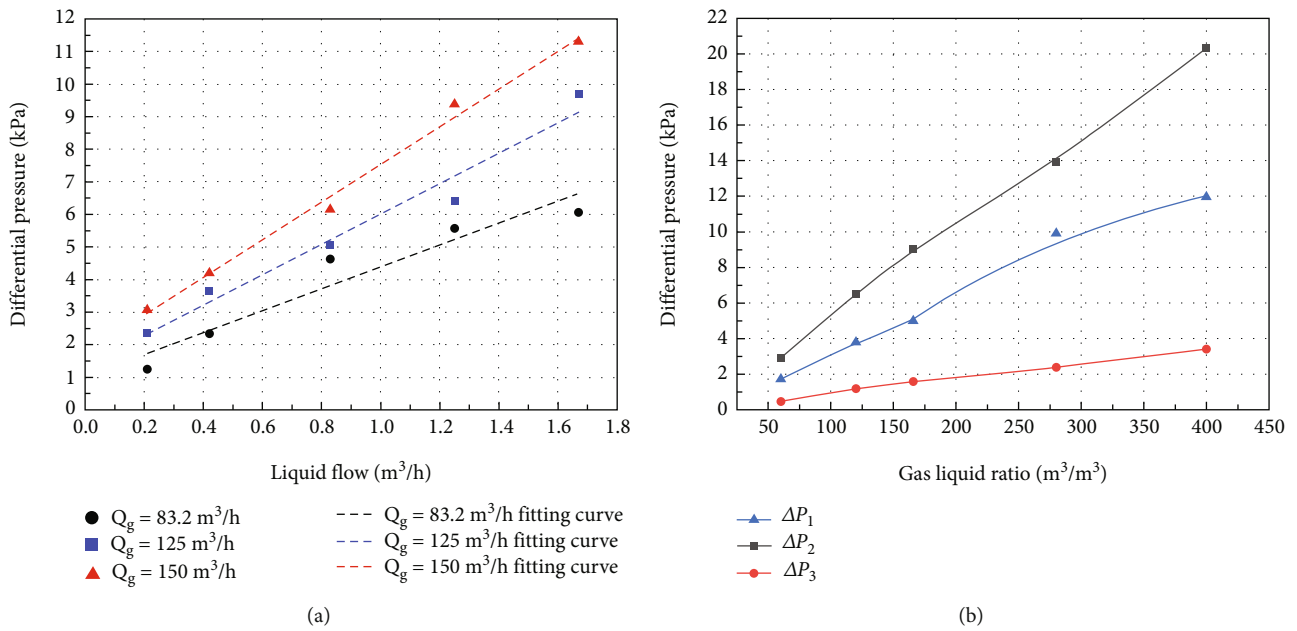


FIGURE 12: (a) Pressure drop variation at different liquid phase flow conditions; (b) differential pressure variation curves at different cross-sections (ΔP_1 sudden contraction structure, ΔP_2 Venturi-tapering section, ΔP_3 Venturi-expansion section).

that an increase in the gas-liquid ratio leads to a significant increase in the total pressure drop at constant pressure conditions. The differential pressure of the gas-liquid mixture passing through the Venturi nozzle is related to the magnitude of the flow rate and increases with increase of the gas-liquid ratio [29, 30].

4.5. Model Building

4.5.1. Venturi Differential Pressure. Based on the experimental and numerical simulation results, the pressure drop cal-

culation model of this device is established. The pressure drop generated by the Venturi nozzle mainly includes an accelerated pressure drop and friction pressure drop [31]. Among them, the acceleration pressure drop accounts for the largest proportion and increases with the increase of the liquid content. The next is the frictional pressure drop, which is mainly generated at the nozzle. The frictional pressure drop increases due to the reduction of the flow channel. The experimental and simulation results show that the frictional pressure drop accounts for a small percentage

of the total pressure drop. Based on the installation location of the ejector and the focus of the study, the frictional pressure drop and the repositioning pressure drop are neglected in this calculation.

The accelerated pressure drop in the axial position of the Venturi [32] can be calculated by the following equation.

$$\Delta P_v = \frac{G_m v_{g,th}}{A\varphi} = \Delta P_2 + \Delta P_3, \quad (17)$$

where the gas velocity in the Venturi throat can be expressed as the following equation.

$$v_{g,th} = 0.135 X_{LM} Fr_g^{1.27} \left(\frac{\rho_l}{\rho_g} \right)^{0.806}, \quad (18)$$

where G_m represents the mass flow rate of the mixture, kg/s; $v_{g,th}$ is the Venturi throat gas velocity, m/s; A represents the cross-sectional area, m²; φ represents the cross-sectional gas content, dimensionless; and X_{LM} and Fr_g represent the Lockhart-Martinelli number and gas Froude number, respectively, dimensionless.

4.5.2. Differential Pressure of Drainage Pipe Inlet. The pressure drop at the inlet of the drainage pipe is mainly caused by the sudden shrinkage of the pipe diameter, as shown in the structure in Figure 2(c). Therefore, in this study, the pressure drop between section 1 and section 2 is investigated using the pressure drop calculation method of the abruptly shrunken pipe. Due to the small experimental pressure, it is assumed that there is no significant change in the density of the gas-liquid phase and no mass exchange.

The continuity equations for the gas and liquid phases on cross-section 1 and cross-section 2 are obtained from the conservation of mass.

$$G_{gs} = \rho_g A_g v_{gs} = \rho_g A_s \varphi_s, \quad (19)$$

$$G_{ls} = \rho_l A_l v_{ls} = \rho_g v_{ls} A_s (1 - \varphi_s), \quad (20)$$

where G_g and G_l represent the mass flow rate of the gas and liquid, respectively, kg/s; A_g and A_l represent the cross-section of the gas and liquid, respectively, m²; φ_s represents the gas content of a section, dimensionless; v_{gs} and v_{ls} represent the flow rate of the gas and liquid of a section, respectively, m/s; and s represents any section of section 1 and section 2.

Since the section is very short and friction is neglected, the sum of the external forces on the two gas-liquid phases along the axial direction is $A_2(P_1 - P_2)$; then, the momentum equation is

$$P_1 - P_2 = \frac{1}{A_2} (G_{g2} v_{g2} + G_{l2} v_{l2} - G_{g1} v_{g1} - G_{l1} v_{l1}). \quad (21)$$

The subscript 1 represents the inlet section of the protruding joint and 2 represents the outlet section of the protruding joint.

From the analysis of simulation results, it is found that the streamline of the gas-liquid mixture is bent downstream of the sudden contraction pipe (Figure 2(c), section t). Therefore, the resistance loss of the sudden contraction pipe is mainly generated from section t to section 2 [33]. Based on the specificity of the structure, it is assumed that the gas content of the drainage pipe is equal to that of section 2; i.e., $\varphi_t = \varphi_2 = \varphi$. From the momentum equation, the pressure drop of the sudden contraction pipe can be calculated as

$$\Delta P_1 = \frac{0.235 G_m}{\rho_l A_1^2} \left[\frac{(1 - \alpha)^2}{1 - \varphi} + \frac{\alpha^2 \rho_l}{\varphi \rho_g} \right], \quad (22)$$

where α is the dryness fraction, dimensionless. G_m is the gas-liquid two-phase mass flow rate, kg/s.

4.5.3. Impacting Tee Differential Pressure. The pressure loss from the impacting tee is calculated according to the following Eq. (23) calculation [34].

$$\Delta P_o = \lambda \frac{Q_m^2}{2A^2 \rho_l} \left[1 + x \left(\frac{\rho_g}{\rho_l} - 1 \right) \right], \quad (23)$$

Where the local resistance factor λ is calculated using the following equation.

$$\lambda = c \lambda_o. \quad (24)$$

The correction factor c is obtained using the empirical equation:

$$c = 1 + 0.75 \left[\frac{x(1-x) \left[1 + \rho_l / \rho_g \right] \sqrt{1 - \rho_g / \rho_l}}{1 + x \left(\rho_l / \rho_g - 1 \right)} \right]. \quad (25)$$

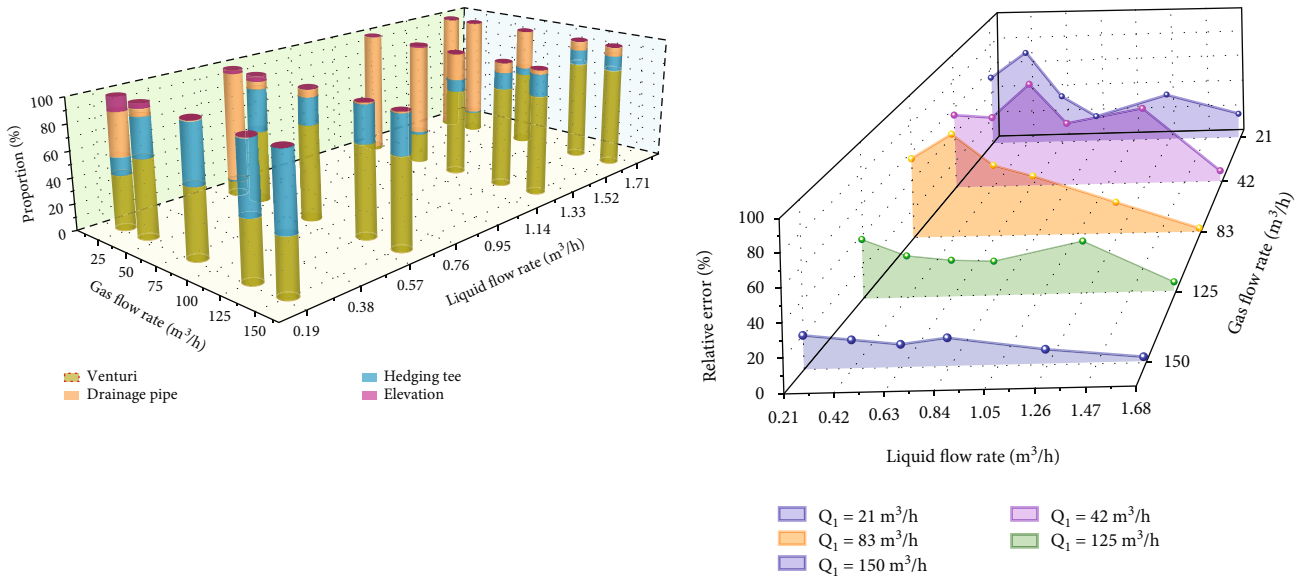
4.5.4. Heavy Pressure Drop. According to the operating principle of the device, the repositioning pressure drop is mainly generated in the rising pipe section of the drainage pipe and the impacting tee. The calculation equation is

$$\Delta P_h = 2 \rho_m g \Delta h. \quad (26)$$

Since the diameter of the drainage pipe is much smaller than the accumulation riser when the gas-liquid mixture enters the drainage pipe, the flow rate of the liquid phase suddenly increases, and when the superficial velocity of the gas-liquid two phases are equal, the slip ratio is 1. Therefore, referring to Eq. (12), the following equation is used to calculate the mixing density.

$$\rho_m = \rho_g \varphi + \rho_l (1 - \varphi). \quad (27)$$

4.6. Accuracy Verification. As per Figure 13(a), it can be seen that under atmospheric conditions, the Venturi nozzle pressure drop has the largest proportion in the total pressure drop, while the heavy pressure drop has the smallest proportion. In small-volume conditions, the pressure drop caused by sudden



(a) Proportion of local pressure drop (b) Comparison of pressure drop calculation error
 FIGURE 13: Comparative analysis of the error of pressure drop calculation under different gas-liquid ratio conditions.

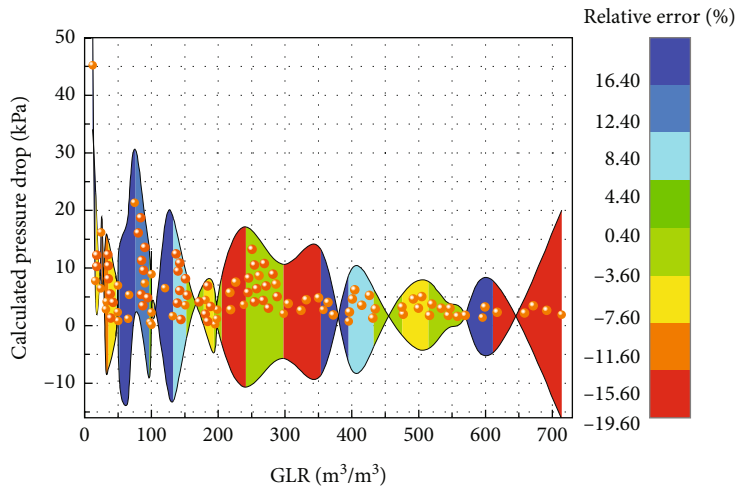


FIGURE 14: Relative error distribution of pressure drop calculation after correction.

changes in the diameter of the drainage pipe is the largest. The pressure drop of the Venturi nozzle increases with the liquid flow rate, and its average proportion is 52.82% of the total pressure drop. In the large liquid volume and small air volume conditions, the pressure drop at the inlet of the drainage pipe produced a maximum percentage of 95.83%.

According to the calculation results, it can be seen that the pressure drop calculation method obtained from this experiment can truly reflect the motion of the fluid. The error of the pressure drop calculation increases gradually with the decrease in the gas flow rate, as shown in Figure 13(b). The relative error is the smallest when the liquid flow rate is 1.67 m³/h. As the gas flow rate decreases gradually, the relative error increases gradually. The gas-liquid rate is small, and the liquid phase is mostly deposited at the bottom of the accumulation riser due to gravity. As

shown in Figure 7(c), the liquid level is higher than the inlet of the drainage pipe. The height difference of the liquid level provides energy for the liquid movement, and the gravitational potential energy is ignored in the calculation. This is the main reason for the large calculation results and the large error in the total pressure drop. When the gas flow rate increases, the Venturi produces a larger proportion of the pressure drop. The calculation accuracy of the total pressure drop depends on the Venturi nozzle. Under a large gas flow rate, the flow rate at the Venturi nozzle changes little, the measured results match the calculated results to a high coincidence, and the calculation error is small.

4.7. Model Correction. To further improve the calculation accuracy of the pressure drop under different gas-liquid ratios, the total pressure drop calculation method of the slug

flow elimination device is optimized based on the pressure drop ratio of different structures. The modified pressure drop calculation method is obtained as follows.

$$\Delta P = 0.804 + 0.957(\Delta P_o + \Delta P_1 + \Delta P_h) + 0.421\Delta P_v^{1.5}. \quad (28)$$

As Figure 14 shows, the pressure drop gradually decreases as the gas-liquid ratio increases. The accuracy of the modified pressure drop calculation method is significantly improved, and the error with the measured pressure drop is kept within 20%, among which 69.31% of the data points are within 10%.

5. Conclusion

According to the motion law of slug flow, the elimination device designed based on the kinetic energy conversion method can better solve the problem of large pressure fluctuations caused by slug flow. In this study, the flow field of the slug flow through the elimination device is analyzed. The energy losses generated during the operation of the device are evaluated. A pressure drop calculation method for this device is developed based on the share of different structures in the total pressure drop. The relative error of the pressure drop model is controlled within 20%, which meets the process production requirements. The optimal and most economical operating range of the device is to maintain the gas-liquid ratio within $120 \text{ m}^3/\text{m}^3$ (under operating conditions). The device can provide stable flow patterns and pressure conditions for gas-liquid two-phase flow measurements for the oil well.

Data Availability

Data can be obtained by contacting the corresponding author (Xingkai Zhang, zhangxingkai001@163.com).

Conflicts of Interest

The authors declare that they have no conflicts of interest.

Acknowledgments

The authors would like to acknowledge the support provided by the National Natural Science Foundation of China (Grant No: 62173049) and the open fund of the Key Laboratory of Exploration Technologies for Oil and Gas Resources (Yangtze University), Ministry of Education of China (Grant: K2021-17).

References

- [1] H. L. Xue, X. Y. He, and H. J. Sun, "Research and application of flow type adjuster in multiphase metering system," *Instrumentation User*, vol. 47, 2018(09), 39-40+44.
- [2] A. Sqw, A. Kwx, and B. Hbka, "Slug flow identification using ultrasound doppler velocimetry - Science Direct," *International Journal of Heat and Mass Transfer*, vol. 148, 2019.
- [3] K. Ran, K. Seungjin, B. Stephen, T. Kirk, and H. Chris, "Experimental investigation of horizontal air-water bubbly-to-slug and bubbly-to-slug transition flows in a 3.81 cm ID pipe," *International Journal of Multiphase Flow*, vol. 94, pp. 137-155, 2017.
- [4] R. Deendarlianto, W. Andinusa, D. Arif, and W. A. Okto, "Experimental study on the hydrodynamic behavior of gas-liquid air-water two-phase flow near the transition to slug flow in horizontal pipes," *International Journal of Heat and Mass Transfer*, vol. 130, pp. 187-203, 2019.
- [5] B. D. Woods, Z. Fan, and T. J. Hanratty, "Frequency and development of slugs in a horizontal pipe at large liquid flows," *International Journal of Multiphase Flow*, vol. 32, no. 8, pp. 902-925, 2006.
- [6] T. K. Mandal, G. Das, and P. K. Das, "An appraisal of liquid-liquid slug flow in different pipe orientations," *International Journal of Multiphase Flow*, vol. 36, no. 8, pp. 661-671, 2010.
- [7] Y. F. Meng, X. K. Zhang, R. Q. Liao, and D. Wang, "A two-parameter measurement method for moisture for the application of forced annular flow," *Journal of Xi'an Jiaotong University*, vol. 54, no. 10, p. 9, 2020.
- [8] W. Zheng, R. Liang, X. Zhang, R. Liao, D. Wang, and L. Huang, "Wet gas measurements of long-throat Venturi tube based on forced annular flow," *Flow Measurement and Instrumentation*, vol. 81, p. 102037, 2021.
- [9] B. T. Yocum, *Offshore riser slug flow avoidance: mathematical models for design and optimization*, SPE European Meeting, OnePetro, London, United Kingdom, 1973.
- [10] L. Xing, H. Yeung, J. Shen, and Y. Cao, "A new flow conditioner for mitigating severe slugging in pipeline/riser system," *International Journal of Multiphase Flow*, vol. 51, pp. 65-72, 2013.
- [11] P. Prickaerts, G. Haandrikman, and R. Henkes, "Two-phase flow behavior for a single flow pipe with a non-symmetric splitter to a dual riser," in *16th International Conference on Multiphase Production Technology*, BHR Group, Cannes, France, 2013.
- [12] S. Cem and J. Tengesdal, "A new technique to eliminate severe slugging in pipeline/riser systems," in *Society of Petroleum Engineers SPE Annual Technical Conference and Exhibition - proceedings of SPE annual technical conference and exhibition*, pp. 633-641, USA, 2000.
- [13] E. Schrama, R. Fernandes, and BHR Group, "The bubble breaker: breaking up slug flow into dispersed bubbly flow using a passive mechanical device," in *12th International Conference on Multiphase Production Technology*, pp. 283-296, Barcelona, Spain, 2005.
- [14] J.-X. Zhang, J.-Y. Zhang, Y. Zhou, Z.-Y.-Y. Cheng, and G.-D. Cao, "Investigation on the performance of a helico-axial multiphase pump under slug flow," *Petroleum Science*, vol. 19, no. 4, pp. 1812-1824, 2022.
- [15] W. Schiferli, J. H. Hansen, B. J. Brasjen, and S. Belfroid, *Experimental Investigation of Terrain Slugging: Formation Mechanism and Potential Mitigation Methods*, TNO, 2013.
- [16] N. Echebarrena, P. D. Mininni, and G. A. Moreno, "Empirical mode decomposition of multiphase flows in porous media: characteristic scales and speed of convergence," *Petroleum Science*, vol. 17, no. 1, pp. 153-167, 2020.
- [17] A. B. Ehinmowo, O. O. Ogunleye, and O. D. Orodu, "Experimental investigation of hydrodynamic slug mitigation potential of an intermittent absorber," *Chemical Engineering Research and Design*, vol. 113, pp. 50-60, 2016.

- [18] L. Xiaoming, *Study on Flow Characteristics of Gas-Liquid Two-Phase and Oil-Gas-Water Three-Phase Section Slug Flow*, China University of Petroleum (East China), Shandong, 2007.
- [19] S. Mo, A. Ashrafiyan, J.-C. Barbier, and S. T. Johansen, "Quasi-3D modelling of two-phase slug flow in pipes," *The Journal of Computational Multiphase Flows*, vol. 6, no. 1, pp. 1–12, 2014.
- [20] S. T. Johansen, S. Mo, E. Meese, J. Oliveira, J. Reyes, and J. Carneiro, "CFD simulations of multiphase flows containing large scale interfaces and dispersed phases with selected production technology applications," in *Offshore Technology Conference*, pp. 2076–2090, Brasil-Rio de Janeiro, Brazil, 2015.
- [21] L. Hongqi, *Theory and Application of Spraying Technology*, Wuhan University Press, Wuhan, 2004.
- [22] Z.-K. Gao, M.-X. Liu, W.-D. Dang, and Q. Cai, "A novel complex network-based deep learning method for characterizing gas-liquid two-phase flow," *Petroleum Science*, vol. 18, 2021.
- [23] G. A. Gregory, "Comments on the prediction of liquid holdup for gas-liquid flow in inclined pipes," *The Canadian Journal of Chemical Engineering*, vol. 52, 1974.
- [24] Y. Taitel and A. E. Dukler, "A model for predicting flow regime transitions in horizontal and near horizontal gas-liquid flow," *AIChE Journal*, vol. 22, no. 1, pp. 47–55, 1976.
- [25] Z. Wang, W. Luo, R. Liao, X. Xie, F. Han, and H. Wang, "Slug flow characteristics in inclined and vertical channels," *Fluid Dynamics & Materials Processing*, vol. 15, no. 5, p. 13, 2019.
- [26] D. Meng, N. D. Jin, Z. K. Gao, Z. Y. Wang, and L. S. Zhai, "Flow pattern and water holdup measurements of vertical upward oil-water two-phase flow in small diameter pipes," *Multiphase Flow*, vol. 41, pp. 91–105, 2012.
- [27] G. A. Gregory, M. K. Nicholson, and K. Aziz, "Correlation of the liquid volume fraction in the slug for horizontal gas-liquid slug flow," *International Journal of Multiphase Flow*, vol. 4, no. 1, pp. 33–39, 1978.
- [28] L. D. Fang, T. Zhang, and Y. Xu, "Slit Venturi-based gas-liquid two-phase flow measurement," *Journal of Sensing Technology*, vol. 8, pp. 1458–1465, 2008.
- [29] F. Al-Ruhaimani, E. Pereyra, C. Sarica, E. Al-Safran, S. Chung, and C. Torres, "A study on the effect of high liquid viscosity on slug flow characteristics in upward vertical flow," *Journal of Petroleum Science & Engineering*, vol. 161, pp. 128–146, 2018.
- [30] M. O. Elobeid, A. Ahmad, A. Al-Sarkhi et al., "Pressure drop measurements in Venturi meters of different beta ratios for oil-water flow experiments," *Arabian Journal for Science and Engineering*, vol. 43, no. 11, pp. 6355–6374, 2018.
- [31] Y. Xu, Y. D. Wang, T. Zhang, and J. H. Wang, "Moisture flow characteristics and structural optimization of Venturi expansion section," *Mechanical Science and Technology*, vol. 37, no. 8, pp. 1272–1279, 2018.
- [32] J. Wang, Y. Xu, T. Zhang, H. Wu, and X. Huo, "A pressure drop model for the annular-mist flow in vertical Venturi," *Journal of Natural Gas Science and Engineering*, vol. 76, pp. 103168–103168, 2020.
- [33] J.-L. Chen, *Petroleum Gas-Liquid Two-Phase Pipe Flow*, Petroleum Industry Press, 1989.
- [34] C.-J. Li and W.-L. Jia, *Multiphase Flow in Oil and Gas Pipes*, Chemical Industry Press, 2015.